

Symmetric Bilinear Regression for Signal Subgraph Estimation

Lu Wang

Department of Statistical Science, Duke University

Zhengwu Zhang

Department of Biostatistics, University of Rochester

David Dunson

Department of Statistical Science, Duke University

May 16, 2022

Abstract

There is increasing interest in learning a set of small outcome-relevant subgraphs in network-predictor regression. The extracted signal subgraphs can greatly improve the interpretation of the association between the network predictor and the response. In brain connectomics, the brain network for an individual corresponds to a set of interconnections among brain regions and there is a strong interest

in linking the brain connectome to human cognitive traits. Modern neuroimaging technology allows a very fine segmentation of the brain, producing very large structural brain networks. Therefore, accurate and efficient methods for identifying a set of small predictive subgraphs become crucial, leading to discovery of key interconnected brain regions related to the trait and important insights on the mechanism of variation in human cognitive traits. We propose a symmetric bilinear model with L_1 penalty to search for small clique subgraphs that contain useful information about the response. A coordinate descent algorithm is developed to estimate the model where we derive analytical solutions for a sequence of conditional convex optimizations. Application of this method on human connectome and language comprehension data shows interesting discovery of relevant interconnections among several small sets of brain regions and better predictive performance than competitors.

Keywords: Brain Connectomics, Coordinate Descent, Network Regression, Symmetric Bilinear Regression, Subgraph Learning, Symmetric Weighted Networks.

1 Introduction

In this article, we study methods for predicting an outcome variable y_i from a network-valued variable W_i , measured on n subjects, where W_i is a $V \times V$ symmetric matrix. In the typical scenario, the number of free elements of

W_i , $V(V - 1)/2$, is much larger than n . In our motivating example, W_i is the weighted adjacency matrix of an individual’s brain structural network, where the brain is segmented into V regions and each entry in W_i denotes the connectivity strength of neural fibers between a pair of regions. The outcome y_i is a cognitive trait of an individual which is a continuous variable. The goal is to select neurologically interpretable subgraphs in the brain connectome, corresponding to a subset of neural connections, that are relevant to the outcome y_i .

One typical approach to this large p small n problem would be a linear regression with some regularization, such as lasso (Tibshirani, 1996), elastic-net regression (Zou and Hastie, 2005) and SCAD (Fan and Li, 2001). These approaches require first flattening out each adjacency matrix into a long vector, which could induce ultra high dimensionality for large networks (Zheng et al., 2015). In addition, the selected connections often do not have any structure in brain connectivity making the results hard to interpret.

Existing feature extraction approaches (Beckmann et al., 2005; Varoquaux et al., 2011; Wang et al., 2017; Zhang et al., 2018a) typically employ a two-stage procedure where some latent representations of the networks are first learnt and a prediction model is trained on the low-dimensional representations. However, such unsupervised approaches have the disadvantage that the low-dimensional structure is extracted to minimize the reconstruction error in network approximation, which may not produce network features that are particularly predictive of the response.

Tensor regression models (Zhou et al., 2013; Zhou and Li, 2014; Hoff, 2015; Li et al., 2016) provide a promising tool for estimating outcome-relevant subgraphs in this situation. Initially proposed for neuroimaging analysis, tensor regression methods can effectively exploit the array-valued covariates to identify regions of interest in brains that are relevant to a clinical response (Zhou et al., 2013). Considering a tensor regression of the response on the matrix-valued network predictor, the set of rank-1 coefficient component matrices naturally selects a collection of clique subgraphs where the edge between any two nodes is predictive of the response.

We propose to use a symmetric bilinear model with L_1 penalty to estimate a set of small signal subgraphs. The model puts symmetry constraints on the coefficient matrix of tensor regression due to the symmetry in predictors - the adjacency matrices of undirected networks are symmetric. In this case, the block-relaxation algorithm (Zhou et al., 2013) of tensor regression cannot be applied. As far as we know, there is no available algorithm for estimating L_1 -penalized symmetric bilinear regression in the literature. We therefore develop an effective algorithm based on the idea of the efficient coordinate descent algorithm (Friedman et al., 2010) of lasso, which involves solving a sequence of conditional convex optimizations.

The rest of the paper is organized as follows. We describe the symmetric bilinear model and the special format of L_1 regularization in the next section. A coordinate descent algorithm for estimation of this model is introduced in Section 3. Section 4 contains a simulation study demonstrating the good

performance of our algorithm in recovering true signal clique subgraphs. We apply the method on brain connectome and cognitive traits data in Section 5 to search for sub-structure in the brain that is relevant to certain cognitive ability. Section 6 concludes.

2 Symmetric Bilinear Regression with L_1 Regularization

The classical linear model relates a vector-valued covariate $\mathbf{x} \in \mathbb{R}^p$ to the conditional expectation of the response y via $E(y \mid \mathbf{x}) = \alpha + \boldsymbol{\beta}^\top \mathbf{x}$. For a matrix-valued covariate $W \in \mathbb{R}^{V \times V}$, one can choose a coefficient matrix B of the same size to capture the effect of each element. Then the linear model has the following form

$$E(y \mid W) = \alpha + \langle B, W \rangle, \quad (1)$$

where $\langle B, W \rangle = \text{trace}(B^\top W) = \text{vec}(B)^\top \text{vec}(W)$. If W is symmetric, the coefficient matrix B should also be symmetric. In this case, B has the same number of parameters, $V(V-1)/2$, as W , which grows quadratically with V and can quickly exceed the sample size n when V is large. For example, typical structural brain networks of size 68×68 require $68 \times 67/2 = 2278$ regression parameters. Hence, the goal is to approximate B with fewer pa-

rameters. If B admits a rank-1 decomposition

$$B = \lambda \boldsymbol{\beta} \boldsymbol{\beta}^\top$$

where $\boldsymbol{\beta} \in \mathbb{R}^V$, the linear part in (1) has the symmetric bilinear form

$$E(y \mid W) = \alpha + \lambda \boldsymbol{\beta}^\top W \boldsymbol{\beta}.$$

A more flexible symmetric bilinear model would be a rank- K approximation to the general coefficient matrix B . Specifically, suppose B admits a rank- K canonical decomposition (CANDECOMP/PARAFAC or CP) (Kolda and Bader, 2009)

$$B = \sum_{h=1}^K \lambda_h \boldsymbol{\beta}_h \boldsymbol{\beta}_h^\top, \quad (2)$$

where $\boldsymbol{\beta}_h \in \mathbb{R}^V$, $\lambda_h \in \mathbb{R}$, $h = 1, \dots, K$. We do not constrain $\{\boldsymbol{\beta}_h\}_{h=1}^K$ to be orthogonal or linearly independent, as such assumptions are often not sensible in practice. The decomposition (2) may not be unique even up to permutation and scaling (Sidiropoulos and Bro, 2000; Liu and Sidiropoulos, 2001; De Lathauwer, 2006). Hence, we introduce an L_1 penalty on the entries of component matrices $\{\lambda_h \boldsymbol{\beta}_h \boldsymbol{\beta}_h^\top\}_{h=1}^K$ to ensure both the identifiability of the model and the sparsity of the coefficient components $\{\lambda_h \boldsymbol{\beta}_h \boldsymbol{\beta}_h^\top\}_{h=1}^K$.

The decomposition (2) leads to a rank- K symmetric bilinear regression

model

$$\begin{aligned}
E(y \mid W) &= \alpha + \left\langle \sum_{h=1}^K \lambda_h \boldsymbol{\beta}_h \boldsymbol{\beta}_h^\top, W \right\rangle \\
&= \alpha + \sum_{h=1}^K \lambda_h \boldsymbol{\beta}_h^\top W \boldsymbol{\beta}_h.
\end{aligned} \tag{3}$$

The loss function of model (3) under L_1 regularization is given by

$$\frac{1}{2n} \sum_{i=1}^n \left(y_i - \alpha - \sum_{h=1}^K \lambda_h \boldsymbol{\beta}_h^\top W_i \boldsymbol{\beta}_h \right)^2 + \gamma \sum_{h=1}^K |\lambda_h| \sum_{u=1}^V \sum_{v < u} |\beta_{hu} \beta_{hv}| \tag{4}$$

where γ is a penalty factor that can be optimised via test data or cross validation in practice. Here we choose to penalize the sum of absolute values of the lower-triangular entries in the matrices $\{\lambda_h \boldsymbol{\beta}_h \boldsymbol{\beta}_h^\top\}_{h=1}^K$ instead of the L_1 norms of the vectors $\{\boldsymbol{\beta}_h\}_{h=1}^K$ for two reasons: (i) this form achieves an adaptive penalty on each β_{hu} (the u -th entry of $\boldsymbol{\beta}_h$) given others; (ii) this form avoids scaling problems between λ_h and $\boldsymbol{\beta}_h$. Regarding (i), by “adaptive penalty” we mean that the penalty factor for β_{hu} in (4) given all the other parameters tends to be high with many nonzero entries in $\boldsymbol{\beta}_h$ and low with few nonzero entries. Refer to Section 3 for technical details on this property. Overall, this conditional adaptive L_1 penalty will lead to sparser matrix estimates $\{\lambda_h \boldsymbol{\beta}_h \boldsymbol{\beta}_h^\top\}_{h=1}^K$ than simply penalizing the L_1 norms of $\{\boldsymbol{\beta}_h\}_{h=1}^K$. Regarding (ii), note that the loss function (4) will not be affected if we change scales for both λ_h and $\boldsymbol{\beta}_h$ simultaneously while leaving the matrix $\lambda_h \boldsymbol{\beta}_h \boldsymbol{\beta}_h^\top$ unchanged. Therefore each component matrix $\lambda_h \boldsymbol{\beta}_h \boldsymbol{\beta}_h^\top$ is identifiable when

minimizing the loss function (4), which is sufficient since the main interest is in the nonzero entries in the coefficient components $\{\lambda_h \boldsymbol{\beta}_h \boldsymbol{\beta}_h^\top\}_{h=1}^K$ instead of $\{\lambda_h\}_{h=1}^K$ and $\{\boldsymbol{\beta}_h\}_{h=1}^K$ separately. Then we do not need to put unit length constraints on $\{\boldsymbol{\beta}_h\}_{h=1}^K$, as often done in CP decomposition (Allen, 2012). However, there will be scaling problems if we only penalize the L_1 norms of $\{\boldsymbol{\beta}_h\}_{h=1}^K$.

The symmetric bilinear model achieves the goal of reducing parameters while maintaining flexibility. Model (3) only has $(1 + K + KV)$ parameters, which is much smaller than the number of parameters, $(1 + V(V - 1)/2)$, in the unstructured linear model (1) when V is large and $K \ll V$. According to Zhou et al. (2013), such a massive reduction in dimensionality provides a reasonable approximation to many low-rank signals. If the true signal edges in the undirected network form several clique subgraphs, the symmetric bilinear model (3) will be much more efficient in requiring many fewer parameters to capture the structure. If this is not the case, model (3) is still flexible at capturing any structure of signal edges in the network with K being large. For example, if we set $K = V(V - 1)/2$ and choose $\{\boldsymbol{\beta}_h\}_{h=1}^K = \{\mathbf{e}_u + \mathbf{e}_v\}_{u < v}$ where $\{\mathbf{e}_u\}_{u=1}^V$ is the standard basis for \mathbb{R}^V , then the symmetric bilinear model (3) becomes unstructured linear regression (1) and equivalent to usual lasso.

The interpretation of the symmetric bilinear model (3) is very appealing in the context of networks. The nonzero entries in each coefficient component matrix $\lambda_h \boldsymbol{\beta}_h \boldsymbol{\beta}_h^\top$ locate a clique subgraph where the edge weight between any two nodes is relevant to the response, and the number of nodes equals the

number of nonzero entries in β_h .

3 Estimation Algorithm

The parameters of the symmetric bilinear model (3) are estimated by minimizing the loss function (4)

$$\min_{\alpha, \{\lambda_h\}, \{\beta_h\}} \frac{1}{2n} \sum_{i=1}^n \left(y_i - \alpha - \sum_{h=1}^K \lambda_h \beta_h^\top W_i \beta_h \right)^2 + \gamma \sum_{h=1}^K |\lambda_h| \sum_{u=1}^V \sum_{v < u} |\beta_{hu} \beta_{hv}|. \quad (5)$$

We consider a coordinate descent step for solving (5). That is, suppose we have estimates for all the parameters but one and wish to partially optimize with respect to the unknown parameter. This procedure is cycled through all the parameters until convergence. Note that the undirected networks of interest do not have self loops, so the diagonal of each adjacency matrix W_i is set to zero below.

3.1 Updates for entries in $\{\beta_h\}_{h=1}^K$

Suppose we want to optimize with respect to β_{hu} , the u -th entry in β_h , given all the other parameters. The problem becomes

$$\min_{\beta_{hu}} L_{\beta, h}(\beta_{hu}) = f_h(\lambda_h, \beta_h) + \left(\gamma |\lambda_h| \sum_{v \neq u} |\beta_{hv}| \right) |\beta_{hu}|, \quad (6)$$

where

$$f_h(\lambda_h, \boldsymbol{\beta}_h) = \frac{1}{2n} \sum_{i=1}^n (e_i^{(h)} - \lambda_h \boldsymbol{\beta}_h^\top W_i \boldsymbol{\beta}_h)^2, \quad (7)$$

and $e_i^{(h)}$ is the partial residual of subject i excluding the fitting from component h ,

$$e_i^{(h)} = y_i - \alpha - \sum_{k \neq h} \lambda_k \boldsymbol{\beta}_k^\top W_i \boldsymbol{\beta}_k.$$

An important remark on (6) is that the penalty factor for $|\beta_{hu}|$, $\gamma |\lambda_h| \sum_{v \neq u} |\beta_{hv}|$, is related to the nonzero entries in $\boldsymbol{\beta}_h$ excluding β_{hu} . Hence β_{hu} is more likely to be shrunk to zero if the current number of nonzero entries in $\boldsymbol{\beta}_h$ is large. This adaptive penalty will lead to a set of sparse vectors $\{\boldsymbol{\beta}_h\}_{h=1}^K$ and hence a set of small signal subgraphs.

Since the diagonal elements of each W_i are all equal to zero, $f_h(\lambda_h, \boldsymbol{\beta}_h)$ is actually a partial quadratic function of β_{hu} given $\{\beta_{hv}\}_{v \neq u}$ and hence a partial convex function of β_{hu} with

$$\frac{\partial f_h}{\partial \beta_{hu}} = -\frac{2\lambda_h}{n} \sum_{i=1}^n \left(e_i^{(h)} - \lambda_h \boldsymbol{\beta}_h^\top W_i \boldsymbol{\beta}_h \right) W_{i[u \cdot]} \boldsymbol{\beta}_h \quad (8)$$

$$\frac{\partial^2 f_h}{\partial \beta_{hu}^2} = \frac{4\lambda_h^2}{n} \sum_{i=1}^n (W_{i[u \cdot]} \boldsymbol{\beta}_h)^2 \geq 0 \quad (9)$$

where $W_{i[u \cdot]}$ is the u -th row of W_i and $W_{i[\cdot u]}$ is the u -th column of W_i below.

To find the optimal β_{hu} , we write (8) as

$$\begin{aligned} \frac{\partial f_h}{\partial \beta_{hu}} = & -\frac{2\lambda_h}{n} \sum_{i=1}^n \left(e_i^{(h)} - \lambda_h \boldsymbol{\beta}_h^\top W_i^{(u)} \boldsymbol{\beta}_h \right) W_{i[u\cdot]} \boldsymbol{\beta}_h \\ & + \frac{4\lambda_h^2}{n} (\boldsymbol{\beta}_h^\top M_u \boldsymbol{\beta}_h) \beta_{hu}, \end{aligned} \quad (10)$$

where $W_i^{(u)}$ is W_i with u -th row and u -th column set to zero, and $M_u = \sum_{i=1}^n W_{i[\cdot u]} W_{i[u\cdot]}$. Let $a_{hu} = 2\lambda_h/n \cdot \sum_{i=1}^n (e_i^{(h)} - \lambda_h \boldsymbol{\beta}_h^\top W_i^{(u)} \boldsymbol{\beta}_h) W_{i[u\cdot]} \boldsymbol{\beta}_h$ and $d_{hu} = 4\lambda_h^2/n \cdot \boldsymbol{\beta}_h^\top M_u \boldsymbol{\beta}_h$. Note that $W_{i[uu]} = 0$, so a_{hu} and d_{hu} do not depend on β_{hu} .

The derivative of the second term in the objective function of (6) with respect to β_{hu} only exists if $\beta_{hu} \neq 0$. Hence

$$\frac{\partial L_{\beta,h}}{\partial \beta_{hu}} = \begin{cases} -a_{hu} + d_{hu}\beta_{hu} + \gamma |\lambda_h| \sum_{v \neq u} |\beta_{hv}|, & \text{if } \beta_{hu} > 0 \\ -a_{hu} + d_{hu}\beta_{hu} - \gamma |\lambda_h| \sum_{v \neq u} |\beta_{hv}|, & \text{if } \beta_{hu} < 0 \end{cases} \quad (11)$$

Simple calculus (Friedman et al., 2007) shows that the solution to (6) has the soft-thresholding form

$$\hat{\beta}_{hu} = \frac{1}{d_{hu}} \text{sign}(a_{hu}) \left(|a_{hu}| - \gamma |\lambda_h| \sum_{v \neq u} |\beta_{hv}| \right)_+. \quad (12)$$

Thus (12) gives the analytical form for coordinate-wise update for $\{\beta_{hu} : h = 1, \dots, K; u = 1, \dots, V\}$.

3.2 Updates for $\{\lambda_h\}_{h=1}^K$

Partial optimization with respect to each λ_h while fixing other parameters, solves the following convex optimization

$$\min_{\lambda_h} L_{\lambda,h}(\lambda_h) = f_h(\lambda_h, \boldsymbol{\beta}_h) + \left(\gamma \sum_{u=1}^V \sum_{v < u} |\beta_{hu} \beta_{hv}| \right) |\lambda_h|. \quad (13)$$

The derivative of $L_{\lambda,h}$ only exists if $\lambda_h \neq 0$ and has a similar form to (11) as

$$\frac{\partial L_{\lambda,h}}{\partial \lambda_h} = \begin{cases} -c_h + b_h \lambda_h + \gamma \sum_{u=1}^V \sum_{v < u} |\beta_{hu} \beta_{hv}|, & \text{if } \lambda_h > 0 \\ -c_h + b_h \lambda_h - \gamma \sum_{u=1}^V \sum_{v < u} |\beta_{hu} \beta_{hv}|, & \text{if } \lambda_h < 0 \end{cases} \quad (14)$$

where $c_h = 1/n \cdot \sum_{i=1}^n \boldsymbol{\beta}_h^\top W_i \boldsymbol{\beta}_h e_i^{(h)}$ and $b_h = 1/n \cdot \sum_{i=1}^n (\boldsymbol{\beta}_h^\top W_i \boldsymbol{\beta}_h)^2$. The coordinate-wise update for each λ_h has the form

$$\hat{\lambda}_h = \frac{1}{b_h} \text{sign}(c_h) \left(|c_h| - \gamma \sum_{u=1}^V \sum_{v < u} |\beta_{hu} \beta_{hv}| \right)_+, \quad h = 1, \dots, K. \quad (15)$$

3.3 Update for α

Given other parameters, the optimal α is

$$\hat{\alpha} = \frac{1}{n} \sum_{i=1}^n \left(y_i - \sum_{h=1}^K \lambda_h \boldsymbol{\beta}_h^\top W_i \boldsymbol{\beta}_h \right). \quad (16)$$

3.4 Other details

This coordinate descent algorithm is guaranteed to converge to a local minimum as each update always decreases the objective function in (5) (Bezdek and Hathaway, 2002). In general, the algorithm should be run from multiple initializations to locate a good local minimum. One important remark is that although the entries in $\{\boldsymbol{\beta}_h\}_{h=1}^K$ and $\{\lambda_h\}_{h=1}^K$ have closed form solution of 0 under sufficiently large penalty factor γ , we cannot initialize them at zero as the results will get stuck at zero. Update form (12) and (15) imply that given others being zero, the optimal β_{hu} or λ_h will also be zero. In fact, we recommend to initialize all the parameters to be nonzero in case some components unexpectedly degenerate at the beginning. In practice, we initialize each $\beta_{hu} \sim U(-1, 1)$ and initialize α and $\{\lambda_h\}_{h=1}^K$ by a least-square regression of y_i on $\{\boldsymbol{\beta}_h^\top W_i \boldsymbol{\beta}_h\}_{h=1}^K$.

Another remark relates to the invariance of loss function (4) under rescaling between λ_h and $\boldsymbol{\beta}_h$. The estimated component matrices $\{\lambda_h \boldsymbol{\beta}_h \boldsymbol{\beta}_h^\top\}_{h=1}^K$ from our algorithm do not depend on the magnitude of initial values for $\{\lambda_h\}_{h=1}^K$ and $\boldsymbol{\beta}_h$ as long as the initial matrices of $\{\lambda_h \boldsymbol{\beta}_h \boldsymbol{\beta}_h^\top\}_{h=1}^K$ remain unchanged.

Considerable speedup is obtained by organizing the iterations around the nonzero parameters – active set, as recommended in Friedman et al. (2010). After a few complete cycles through all the parameters, we iterate on only the active set till convergence. The general procedure of the coordinate descent algorithm is summarized in Algorithm 1.

Algorithm 1 Coordinate descent for L_1 -penalized symmetric bilinear model

- 1: **Input:** Adjacency matrices W_i of size $V \times V$, outcome y_i , $i = 1, \dots, n$; rank K , penalty factor γ , tolerance $\epsilon \in \mathbb{R}_+$.
 - 2: **Output:** Estimates of α , $\{\lambda_h\}_{h=1}^K$, $\{\beta_h\}_{h=1}^K$.
 - 3: Initialize $\{\beta_h\}_{h=1}^K$ at nonzero random vectors; initialize α and $\{\lambda_h\}_{h=1}^K$ by a least-square regression of y_i on $\{\beta_h^\top W_i \beta_h\}_{h=1}^K$.
 - 4: **repeat**
 - 5: **for** $h = 1 : K$ **do**
 - 6: **for** $u = 1 : V$ **do**
 - 7: Update β_{hu} by (12)
 - 8: **end for**
 - 9: **end for**
 - 10: **for** $h = 1 : K$ **do**
 - 11: Update λ_h by (15)
 - 12: **end for**
 - 13: Update α by (16)
 - 14: **until** relative change of objective function (5) $< \epsilon$
-

4 Simulation Study

In this experiment, we compare the performance of recovering true signal subgraphs among lasso, tensor network principal components analysis (TN-PCA) and symmetric bilinear regression with L_1 penalty (SBL). TN-PCA (Zhang et al., 2018a) is an unsupervised dimension reduction method, which approximates a semi-symmetric 3-way tensor \mathcal{W} by a sum of rank-one tensors:

$$\mathcal{W} \approx \sum_{k=1}^K d_k \mathbf{v}_k \circ \mathbf{v}_k \circ \mathbf{u}_k, \quad (17)$$

where \mathcal{W} is a concatenation of symmetric (demeaned) adjacency matrices $\{W_i\}_{i=1}^n$, d_k is a positive scaling parameter, \circ denotes the outer product, \mathbf{v}_k

is a $V \times 1$ vector of unit length that stores the PC score for each node in component k , and \mathbf{u}_k is a $n \times 1$ vector of unit length that stores the PC score for each network in component k . Zhang et al. (2018a) also put orthogonality constraints on the component vectors \mathbf{v}_k 's but leave the vectors \mathbf{u}_k 's unconstrained. The TN-PCA (17) embeds the $V \times V$ undirected networks $\{W_i\}_{i=1}^n$ into a low dimensional $n \times K$ matrix $U = (\mathbf{u}_1, \dots, \mathbf{u}_K)$, where each row i represents a $1 \times K$ embedded vector for network i . When $K < n$, we can study the relationship between the network W_i and an outcome y_i via a simple linear regression on the low dimensional embeddings U . The set of rank-one matrices $\{\mathbf{v}_k \mathbf{v}_k^\top\}_{k=1}^K$ can be viewed as basis networks and the ones corresponding to the significant components in the regression of y are selected as signal sub-networks.

We simulate a synthetic dataset consisting of 100 pairs of observations $\{(W_i, y_i) : i = 1, \dots, 100\}$ as follows. Each pair consists of a 20×20 adjacency matrix W_i and a scalar $y_i \in \mathbb{R}$. Specifically, each network W_i is generated from a set of basis subgraphs with an individual loading vector as

$$W_i = \sum_{h=1}^{10} \lambda_{ih} \mathbf{q}_h \mathbf{q}_h^\top + \Delta_i, \quad (18)$$

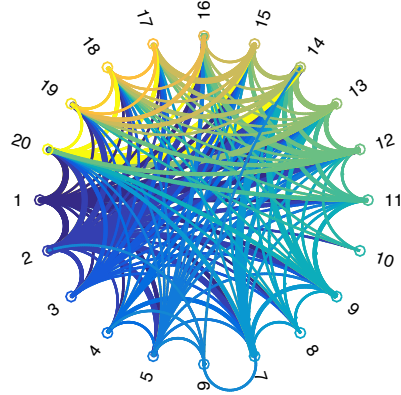


Figure 1: Overlay of 10 basis subgraphs corresponding to $\{\mathbf{q}_h \mathbf{q}_h^\top\}_{h=1}^{10}$.

where $\mathbf{q}_h \in \{0, 1\}^{20}$ is a random binary vector with $\|\mathbf{q}_h\|_0 = h + 1$, $h = 1, \dots, 10$.

The loadings $\{\lambda_{ih}\}$ in (18) are generated independently from $N(0, 1)$. Δ_i is a symmetric 20×20 noise matrix with each entry $\Delta_{i[uv]} \sim N(0, 0.1^2)$, $u > v$. This generating process produces dense networks with complex structure. Figure 1 visualizes the 10 basis subgraphs superimposed together.

The response y_i is generated by

$$y_i = \mathbf{q}_1^\top W_i \mathbf{q}_1 + \mathbf{q}_2^\top W_i \mathbf{q}_2 + \mathbf{q}_3^\top W_i \mathbf{q}_3 + \varepsilon_i, \quad (19)$$

where $\varepsilon_i \sim N(0, \sigma^2)$. We display the results for two noise levels: $\sigma = 10\%$ and 100% of the standard deviation of the conditional mean $E(y_i | W_i)$, respectively. The generating process (19) indicates that the true signal subgraphs that are relevant to y_i are three clique subgraphs corresponding to $\{\mathbf{q}_h \mathbf{q}_h^\top : h = 1, 2, 3\}$ as displayed in Figure 2.

4.1 High signal-to-noise ratio

In this case, we set the noise level $\sigma = 10\%$ of the standard deviation of the conditional mean $E(y_i | W_i)$ in the generating process (19).

The input parameters of Algorithm 1 for SBL are set as follows. We recommend to choose a large K and zero out the empty components adaptively in the result. K is set at 5 and the tolerance $\epsilon = 10^{-5}$ in this simulation study. It is easy to find a *roughly* smallest value γ_{\max} for which $\{\boldsymbol{\beta}_h\}_{h=1}^K$ and

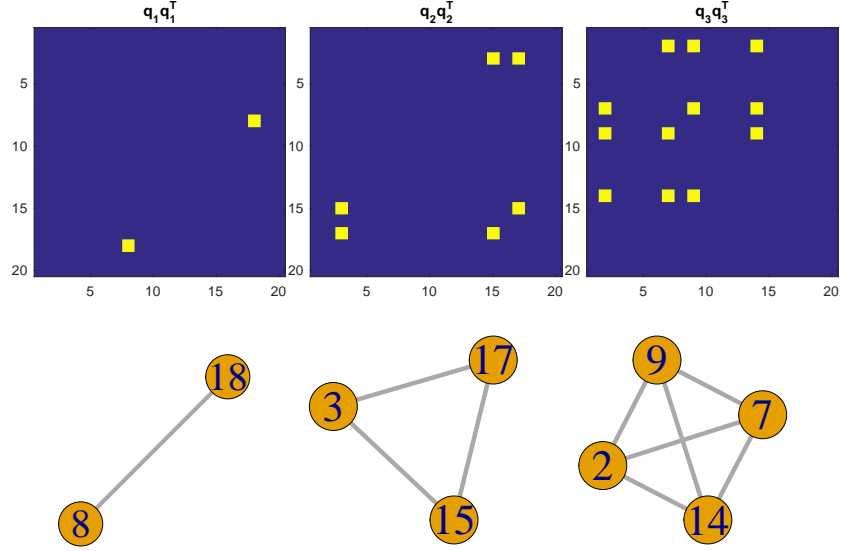


Figure 2: True signal subgraphs in simulation: $\{\mathbf{q}_h \mathbf{q}_h^\top : h = 1, 2, 3\}$ (upper panel) and the corresponding clique subgraphs (lower panel).

$\{\lambda_h\}_{h=1}^K$ become zero. We set $\gamma_{\min} = 0.01\gamma_{\max}$ and choose a sequence of 50 equally spaced γ values on the logarithmic scale.

The dataset is split into a training set and a test set with each consisting of 50 observations, for tuning the L_1 penalty factor. Figure 3 displays the mean squared error (MSE) on test data across different values of the L_1 penalty factor for lasso and SBL respectively. As can be seen, the out-of-sample MSE does not vary much with small values of the penalty factor for both models. Therefore we set the optimal L_1 penalty factor at the largest possible value that produces small MSE (e.g. less than 3% of the maximum MSE when all the parameters are zero in this case) for both models as indicated in Figure 3.

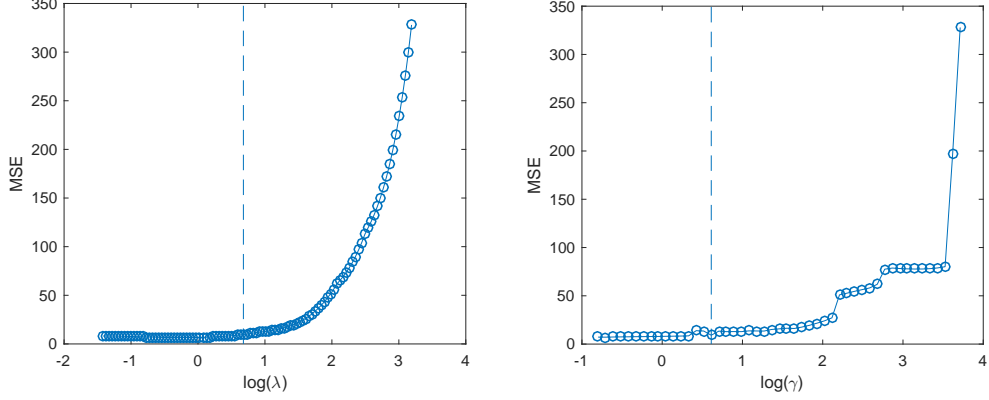


Figure 3: Out-of-sample MSE from lasso (left) and SBL (right) under high signal-to-noise ratio. The vertical line in either plot indicates the selected value of the L_1 penalty factor in coefficient estimation.

The estimated coefficients from lasso are displayed in the lower-triangular matrix in Figure 4 with the true coefficients in the upper-triangular. As can be seen, lasso misses some true signal edges and it is not straightforward to identify meaningful structure among the selected edges.

For the linear regression based on TN-PCA, we set the rank $K = 20$ in (17), which explains approximately 100% of the variation in the networks. The MSE on test data from TN-PCA is 19.46, much higher than the MSE at the optimal L_1 penalty factor,

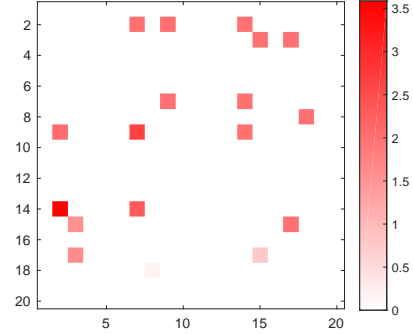


Figure 4: Estimated coefficients from lasso (lower-triangular) under high signal-to-noise ratio and the true coefficients for each edge of the network (upper-triangular).

9.67 for lasso and 9.17 for SBL. The linear regression on the network PC scores shows that all the 20 components are significant at the 5% significance level, which is noninformative of the subgraphs relevant to y since all the basis networks $\{\mathbf{v}_k \mathbf{v}_k^\top\}_{k=1}^{20}$ are dense.

The estimated coefficient components for $\{\lambda_h \boldsymbol{\beta}_h \boldsymbol{\beta}_h^\top\}_{h=1}^5$ from SBL as well as the selected subgraphs are displayed in Figure 5, where only 4 out of 5 components are nonempty. Figure 5 shows that our model recovers all the true signal subgraphs – a single edge, a triangle and a 4-node clique, though the component $\lambda_4 \boldsymbol{\beta}_4 \boldsymbol{\beta}_4^\top$ repeatedly selects an edge in the true triangle signal.

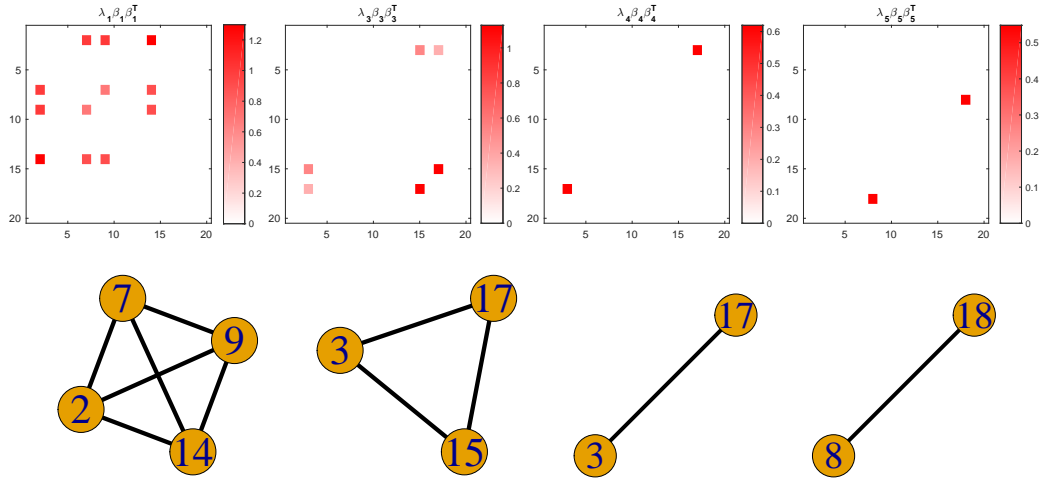


Figure 5: Estimated nonzero coefficient components $\{\lambda_h \boldsymbol{\beta}_h \boldsymbol{\beta}_h^\top\}$ from SBL (upper) and their selected subgraphs (lower) under high signal-to-noise ratio.

The procedure described above is repeated 100 times, where each time we generate a synthetic dataset based on (18) and (19), and record the out-of-sample MSE (at the optimal L_1 penalty factor for lasso and SBL), the true

positive rate (TPR) representing the proportion of true signal edges that are correctly identified, and the false positive rate (FPR) representing the proportion of non-signal edges that are falsely identified, for lasso, TN-PCA and SBL. Table 1 displays the mean and standard deviation (sd) of the MSE, TPR and FPR for the three methods, which shows that SBL has the highest average TPR, though a bit higher MSE than that of TN-PCA and a bit higher FPR than that of lasso on average.

Table 1: Mean and sd of the MSE, TPR and FPR across 100 simulations under high signal-to-noise ratio.

	MSE	TPR	FPR
lasso	10.98±4.40	0.837±0.138	0.002±0.005
TN-PCA	10.04±4.66	0.449±0.499	0.449±0.499
SBL	10.08±4.51	0.848±0.169	0.005±0.007

4.2 Low signal-to-noise ratio

In this case, the noise level $\sigma = 100\%$ of the standard deviation of the conditional mean $E(y_i | W_i)$ in the generating process (19).

Figure 6 displays the MSE on test data versus the L_1 penalty factor for lasso and SBL respectively. We set the optimal L_1 penalty factor for either model at the value that produces the minimum out-of-sample MSE as indicated in Figure 6.

The estimated coefficients from lasso are displayed in the lower-triangular matrix in Figure 7, which shows that lasso misses many true signal edges and

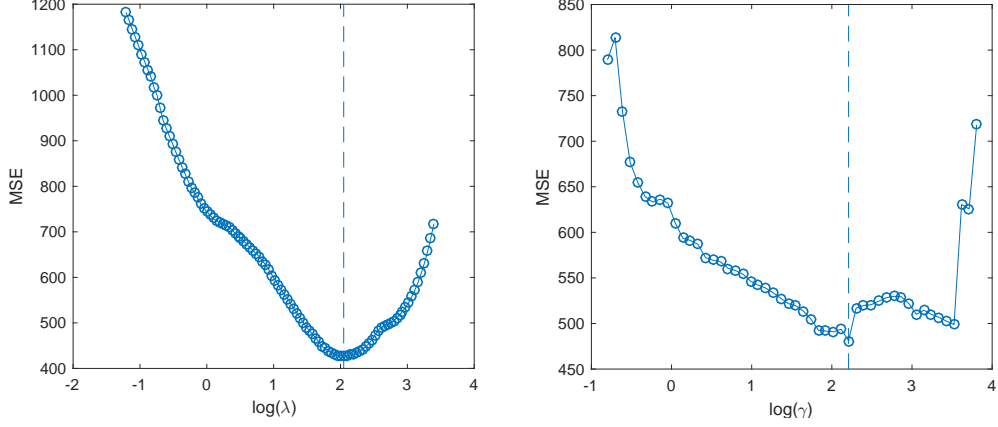


Figure 6: Out-of-sample MSE from lasso (left) and SBL (right) under low signal-to-noise ratio. The vertical line in either plot indicates the selected value of the L_1 penalty factor in coefficient estimation.

selects a false edge with very large coefficient in this case.

The MSE on test data from TN-PCA is 1249.1, much higher than the minimum MSE, 427.5 for lasso and 481.1 for SBL. The linear regression on the network PC scores shows that none of the 20 components are significant in this case.

SBL only selects two nonzero coefficient components $\{\lambda_h \boldsymbol{\beta}_h \boldsymbol{\beta}_h^\top\}$ out of 5 in this case, which are displayed in Figure 8 along with the selected subgraphs. Figure 8 shows that our model perfectly

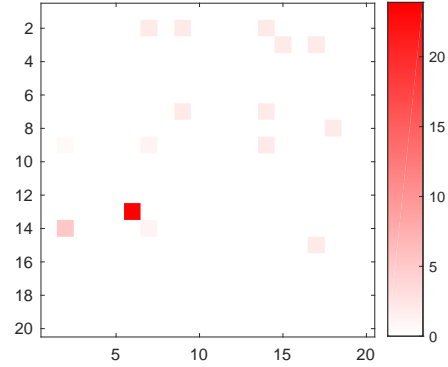


Figure 7: Estimated coefficients from lasso (lower-triangular) under low signal-to-noise ratio and the true coefficients for each edge of the network (upper-triangular).

recovers one true signal subgraph – the 4-node clique, though partially recovers the triangle signal by identifying one edge and misses the single-edge signal.

The procedure described above is again repeated 100 times and Table 2 displays the mean and sd of the out-of-sample MSE, TPR and FPR for the three methods. Table 2 shows that SBL has the lowest out-of-sample MSE and highest TPR on average in this case, though a bit higher average FPR than that of lasso.

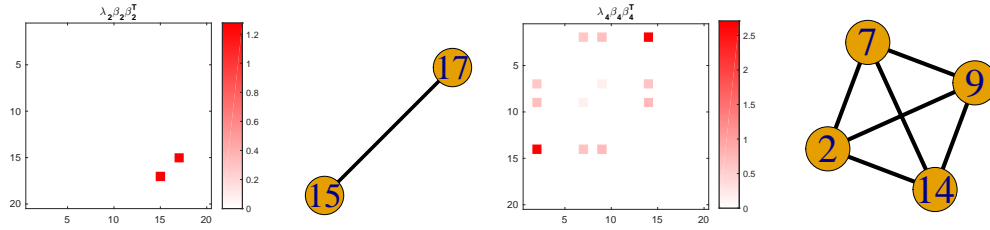


Figure 8: Estimated nonzero coefficient components $\{\lambda_h \beta_h \beta_h^\top\}$ from SBL and their selected subgraphs under low signal-to-noise ratio.

Table 2: Mean and sd of the MSE, TPR and FPR across 100 simulations under low signal-to-noise ratio.

	MSE	TPR	FPR
lasso	448.3±195.3	0.445±0.141	0.025±0.037
TN-PCA	624.0±287.8	0.060±0.239	0.060±0.238
SBL	393.7±159.2	0.539±0.210	0.029±0.038

5 Application

We applied our method to the Human Connectome Project (HCP) dataset (Van Essen et al., 2012), exploring the association between the brain connectome and two cognitive abilities, auditory language comprehension ability and oral reading ability. The dataset contains dMRI data for 1065 subjects and for each subject, a weighted brain network of fiber counts among 68 regions was constructed by a state-of-the-art dMRI processing pipeline (Zhang et al., 2018b).

5.1 Picture Vocabulary Data

The HCP dataset contains age-adjusted scale scores of the subjects in a picture vocabulary (PV) test where respondents are presented with an audio recording of a word and four photographic images on the computer screen and are asked to select the picture that most closely matches the meaning of the word.

We first compare the predictive performance for the PV scores among lasso, TN-PCA and SBL. The dataset is partitioned into a training set of 565 subjects and a test set of 500 subjects. We set $K = 10$ for SBL. Five initializations are enough for Algorithm 1 to produce robust estimates for this dataset. The MSEs of PV scores on test data from SBL under different values of the L_1 penalty factor γ are shown in Figure 9. The optimal γ is set at the value that produces the smallest MSE, which is smaller than the

minimum MSE of lasso, indicating better predictive performance. We set the rank $K = 68$ in TN-PCA, which explains approximately 93% of the variation in the brain networks. The out-of-sample MSE of TN-PCA is 222.1, which is higher than the minimum MSE of SBL as indicated in Figure 9. The linear regression of the PV scores on the low-dimensional embeddings of the brain networks shows that none of the 68 components are significant at the 5% significance level.

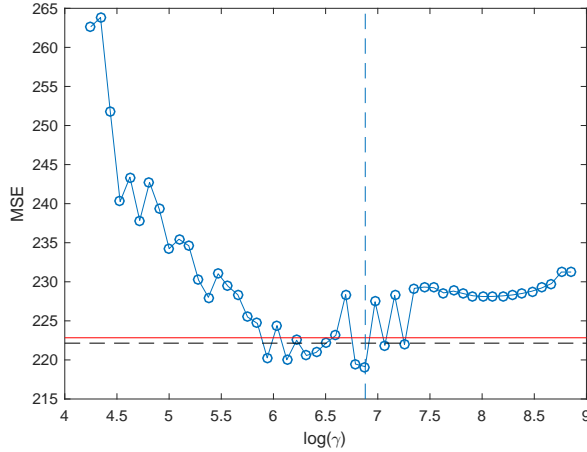


Figure 9: Out-of-sample MSE of SBL on picture vocabulary data. The dashed vertical line indicates the selected value of γ in inference; the red horizontal line indicates the minimum MSE of lasso; the black horizontal line indicates the MSE of TN-PCA.

The estimated coefficients from lasso and the structural connections in the brain corresponding to the nonzero coefficients are displayed in Figure 10. As can be seen, these identified connections lack meaningful structure and are difficult to justify neurologically.

For L_1 -penalized symmetric bilinear regression, only 6 out of 10 coefficient

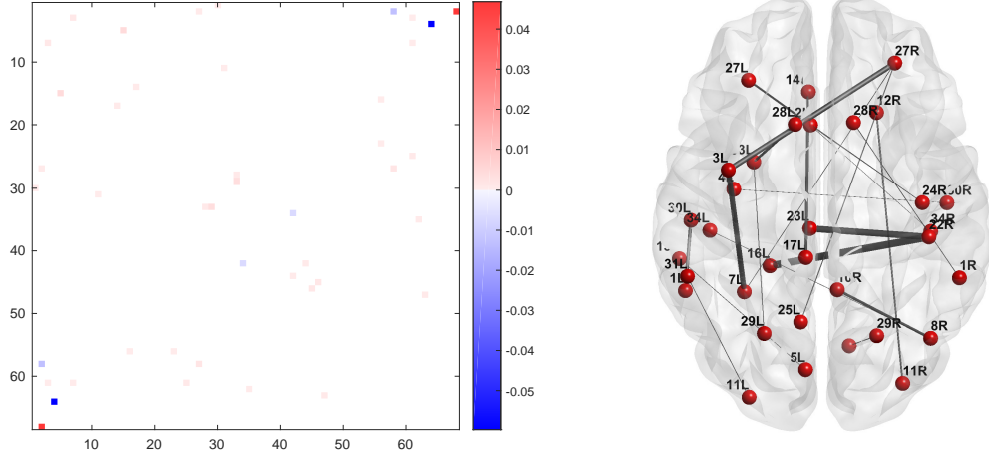


Figure 10: Estimated coefficients from lasso in matrix form (left) and the structural connections in the brain corresponding to nonzero coefficients (right). The thickness of each edge is proportional to the average fiber count between the pair of regions.

component matrices $\{\lambda_h \boldsymbol{\beta}_h \boldsymbol{\beta}_h^\top\}_{h=1}^K$ have nonzero entries, implying $K = 10$ is large enough to capture all the signal subgraphs for this dataset. The estimated nonzero component matrices and their corresponding structural connections in the brain are displayed in Figure 11, which shows that SBL locates multiple simple subgraphs in the brain that may form some anatomical circuits in linguistic processing of sound to meaning. Three subgraphs in Figure 11 only contain a single connection verifying the flexibility of the model. We also observe that some brain regions repeatedly appear in the subgraphs in Figure 11, which may indicate important roles of these regions in auditory comprehension. For example, $27L$, $27R$ (left and right superior frontal gyrus), $7L$ (left inferior parietal gyrus) and $29L$ (left superior temporal

gyrus) are among activated regions when shifting from listening to meaningless pseudo sentences to listening to meaningful sentences (Saur et al., 2008; Dronkers, 2011). Figure 11 also shows that most estimated coefficients of the strengths of these signal connections are positive, implying that stronger neural connections among these regions are expected to lead to higher auditory comprehension ability. These identified anatomical sub-networks in the brain are consistent with the notion that auditory language processing is a complex process, which is the product of the coordinated activities of several brain regions.

5.2 Reading Recognition Data

The HCP dataset also contains the age-adjusted scale scores of the subjects in an oral reading recognition (RR) test where participants were scored on reading and pronouncing letters and words. We apply our method to find sub-networks in the brain connectome relevant to oral reading ability. Following the same procedure of partitioning data as in Section 5.1, we compare the predictive performance for the RR scores among lasso, TN-PCA and SBL. The minimum out-of-sample MSE of SBL is 201.8, which is smaller than that of lasso, 205.9. Although TN-PCA obtains the smallest MSE, 194.7, in this case, the resulting 16 significant components select all the connections in the brain network.

In this case, SBL selects 7 non-empty components $\{\lambda_h \boldsymbol{\beta}_h \boldsymbol{\beta}_h^\top\}$ out of 10 with penalty factor γ set at the optimal value. The subgraphs of brain con-

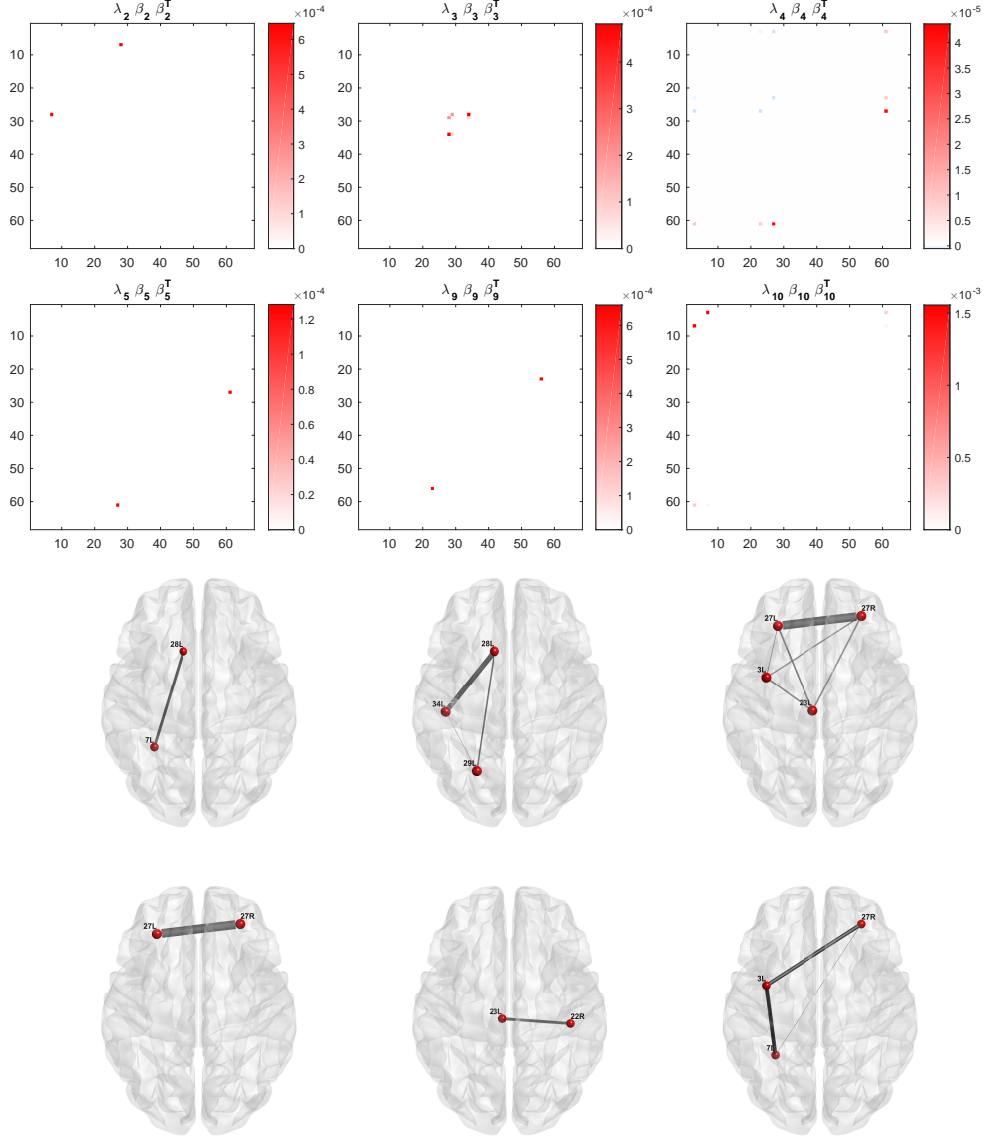


Figure 11: Estimated nonzero component matrices $\{\lambda_h \beta_h \beta_h^\top\}$ for picture vocabulary data (upper) and their selected subgraphs in the brain (lower). The thickness of each edge is proportional to the average fiber count between the pair of brain regions.

nectome corresponding to these nonzero components are displayed in Figure 12. We notice that a triangle subgraph repeatedly appears in these subgraphs, consisting of three regions: 27L (left superior frontal), 23L (left precentral) and 22R (right posterior cingulate). This triangle subgraph may form a core anatomical circuit in the phonological reading pathway. These regions agree with the findings in neuroscience that the superior frontal gyrus is associated with word reading (Cloutman et al., 2011), left precentral gyrus is involved in phonological output (Safi et al., 2016) and the posterior cingulate cortex is associated with language comprehension (Smallwood et al., 2013).

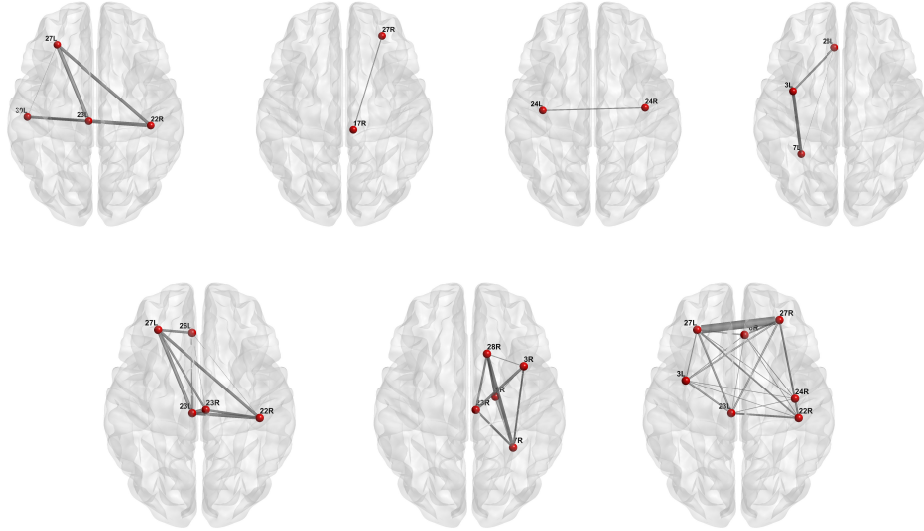


Figure 12: The selected subgraphs in the brain relevant to oral reading ability. The thickness of each edge is proportional to the average fiber count between the pair of brain regions.

6 Conclusion

In summary, the symmetric bilinear model is a useful tool in analyzing the relationship between an outcome and a network-predictor, which produces much more interpretable results than unstructured regression does, while maintaining competitive predictive performance. We develop an effective coordinate descent algorithm for L_1 -penalized symmetric bilinear regression which outputs a set of small outcome-relevant subgraphs. Our method contributes to an insightful understanding of the sub-structure of networks that is relevant to the response and has wide applications in various fields such as neuroscience, internet mapping and social networks. Although we have focused on a continuous response, the methods are straightforward to adapt to classification problems and count responses by a simple modification of the goodness-of-fit component of the loss function.

Supplementary Material

The Matlab code for implementing the coordinate descent algorithm can be found in <https://github.com/wangronglu/Symmetric-Bilinear-Regression>

Acknowledgements

We would like to thank support for this project from Army Research Institute (ARI grant W911NF-16-1-0544).

References

- Allen, G. (2012). Sparse higher-order principal components analysis. In *Artificial Intelligence and Statistics*, pages 27–36.
- Beckmann, C. F., DeLuca, M., Devlin, J. T., and Smith, S. M. (2005). Investigations into resting-state connectivity using independent component analysis. *Philosophical Transactions of the Royal Society B: Biological Sciences*, 360(1457):1001–1013.
- Bezdek, J. C. and Hathaway, R. J. (2002). Some notes on alternating optimization. In *AFSS International Conference on Fuzzy Systems*, pages 288–300. Springer.
- Cloutman, L. L., Newhart, M., Davis, C. L., Heidler-Gary, J., and Hillis, A. E. (2011). Neuroanatomical correlates of oral reading in acute left hemispheric stroke. *Brain and Language*, 116(1):14–21.
- De Lathauwer, L. (2006). A link between the canonical decomposition in multilinear algebra and simultaneous matrix diagonalization. *SIAM Journal on Matrix Analysis and Applications*, 28(3):642–666.
- Dronkers, N. F. (2011). The neural architecture of the language comprehension network: converging evidence from lesion and connectivity analyses. *Frontiers in Systems Neuroscience*, 5:1–20.
- Fan, J. and Li, R. (2001). Variable selection via nonconcave penalized like-

- likelihood and its oracle properties. *Journal of the American statistical Association*, 96(456):1348–1360.
- Friedman, J., Hastie, T., Höfling, H., Tibshirani, R., et al. (2007). Pathwise coordinate optimization. *The Annals of Applied Statistics*, 1(2):302–332.
- Friedman, J., Hastie, T., and Tibshirani, R. (2010). Regularization paths for generalized linear models via coordinate descent. *Journal of Statistical Software*, 33(1):1–22.
- Hoff, P. D. (2015). Multilinear tensor regression for longitudinal relational data. *The Annals of Applied Statistics*, 9(3):1169.
- Kolda, T. G. and Bader, B. W. (2009). Tensor decompositions and applications. *SIAM review*, 51(3):455–500.
- Li, Z., Suk, H.-I., Shen, D., and Li, L. (2016). Sparse multi-response tensor regression for alzheimer’s disease study with multivariate clinical assessments. *IEEE Transactions on Medical Imaging*, 35(8):1927–1936.
- Liu, X. and Sidiropoulos, N. D. (2001). Cramér-rao lower bounds for low-rank decomposition of multidimensional arrays. *IEEE Transactions on Signal Processing*, 49(9):2074–2086.
- Safi, D., Béland, R., Nguyen, D. K., Pouliot, P., Mohamed, I. S., Vannasing, P., Tremblay, J., Lassonde, M., and Gallagher, A. (2016). Recruitment of the left precentral gyrus in reading epilepsy: a multimodal neuroimaging study. *Epilepsy & Behavior Case Reports*, 5:19–22.

- Saur, D., Kreher, B. W., Schnell, S., Kümmerer, D., Kellmeyer, P., Vry, M.-S., Umarova, R., Musso, M., Glauche, V., Abel, S., et al. (2008). Ventral and dorsal pathways for language. *Proceedings of the National Academy of Sciences*, 105(46):18035–18040.
- Sidiropoulos, N. D. and Bro, R. (2000). On the uniqueness of multilinear decomposition of n-way arrays. *Journal of Chemometrics*, 14(3):229–239.
- Smallwood, J., Gorgolewski, K. J., Golchert, J., Ruby, F. J., Engen, H. G., Baird, B., Vinski, M., Schooler, J., and Margulies, D. S. (2013). The default modes of reading: modulation of posterior cingulate and medial prefrontal cortex connectivity associated with comprehension and task focus while reading. *Frontiers in Human Neuroscience*, 7:734–743.
- Tibshirani, R. (1996). Regression shrinkage and selection via the lasso. *Journal of the Royal Statistical Society. Series B (Methodological)*, 58(1):267–288.
- Van Essen, D. C., Ugurbil, K., Auerbach, E., Barch, D., Behrens, T., Bucholz, R., Chang, A., Chen, L., Corbetta, M., Curtiss, S. W., et al. (2012). The human connectome project: a data acquisition perspective. *Neuroimage*, 62(4):2222–2231.
- Varoquaux, G., Gramfort, A., Pedregosa, F., Michel, V., and Thirion, B. (2011). Multi-subject dictionary learning to segment an atlas of brain

- spontaneous activity. In *Biennial International Conference on Information Processing in Medical Imaging*, pages 562–573. Springer.
- Wang, L., Zhang, Z., and Dunson, D. (2017). Common and individual structure of multiple networks. *arXiv preprint arXiv:1707.06360*.
- Zhang, Z., Allen, G., Zhu, H., and Dunson, D. (2018a). Relationships between human brain structural connectomes and traits. *bioRxiv*, page 256933.
- Zhang, Z., Descoteaux, M., Zhang, J., Girard, G., Chamberland, M., Dunson, D., Srivastava, A., and Zhu, H. (2018b). Mapping population-based structural connectomes. *NeuroImage*, 172:130–145.
- Zheng, D., Mhembere, D., Burns, R., Vogelstein, J., Priebe, C. E., and Szalay, A. S. (2015). Flashgraph: processing billion-node graphs on an array of commodity ssds. In *Proceedings of the 13th USENIX Conference on File and Storage Technologies*, pages 45–58.
- Zhou, H. and Li, L. (2014). Regularized matrix regression. *Journal of the Royal Statistical Society: Series B (Statistical Methodology)*, 76(2):463–483.
- Zhou, H., Li, L., and Zhu, H. (2013). Tensor regression with applications in neuroimaging data analysis. *Journal of the American Statistical Association*, 108(502):540–552.

Zou, H. and Hastie, T. (2005). Regularization and variable selection via the elastic net. *Journal of the Royal Statistical Society: Series B (Statistical Methodology)*, 67(2):301–320.